Proc. Natl. Acad. Sci. USA
Vol. 94, pp. 14725–14729, December 1997
Medical Sciences

In vivo NMR and MRI using injection delivery of laser-polarized xenon

(xenon injection/optical pumping)

B. M. GOODSON*, Y.-Q. SONG*, R. E. TAYLOR*, V. D. SCHEPKIN*, K. M. BRENNAN*, G. C. CHINGAS*, T. F. BUDINGER*†, G. NAVON*‡, AND A. PINES*§

*Lawrence Berkeley National Laboratory and University of California, Berkeley, CA 94720; and †Department of Radiology, University of California, San Francisco, CA 94143

Contributed by Alexander Pines, October 7, 1997

ABSTRACT **Because xenon NMR is highly sensitive to the local environment, laser-polarized xenon could be a unique probe of living tissues. Realization of clinical and medical science applications beyond lung airspace imaging requires methods of efficient delivery of laser-polarized xenon to tissues, because of the short spin-lattice relaxation times and relatively low concentrations of xenon attainable in the body. Preliminary results from the application of a polarized xenon injection technique for *in vivo* ^{129}Xe NMR/MRI are extrapolated along with a simple model of xenon transit to show that the peak local concentration of polarized xenon delivered to tissues by injection may exceed that delivered by respiration by severalfold.**

In certain systems, the angular momentum of circularly polarized light can be transferred to nuclear spins by optical pumping (OP) (1–3), thus increasing the NMR sensitivity by four to five orders of magnitude. This potential for enormous signal enhancement has been the driving force behind the study of "polarized" noble gases for possible clinical and biomedical applications. MRI of polarized ^{129}Xe and ^{3}He in the gas phase has already been utilized to image the void spaces in lungs (4–13), the oral cavity (14), and materials (15). The sensitivity enhancement obtained through OP well outweighs the loss in signal suffered from imaging low-density gas-phase media.

Because of the sensitivity of the NMR parameters of ^{129}Xe to its environment (16) and its safety for medical applications (17), it is hoped that dissolved polarized xenon could serve as a probe of tissues and blood flow in living organisms. Recent *in vivo* work in this direction includes imaging of xenon in the brain¶ and xenon NMR of blood and other tissues following respiration of polarized xenon by laboratory animals (9) and humans (13).

One of the major challenges for the application of dissolved polarized xenon for *in vivo* studies is its efficient delivery to the blood and tissues while maintaining its large nonequilibrium spin polarization. With current respiration methods (4–13), the dissolved xenon is diluted throughout the body via blood flow from the lungs; furthermore, because the spin-lattice relaxation time (T_1^{Xe}) of xenon in tissues is generally short (18) [e.g., ≈5 s in blood (19)], loss of xenon polarization can occur in transit before a significant concentration can accumulate in tissues. In previous work (19), a polarized xenon injection technique was developed and used to perform *in vitro* magnetic resonance (MR) studies. In this paper, the feasibility of using polarized xenon injection for *in vivo* studies is demonstrated. ^{129}Xe NMR and MRI were performed following direct intramuscular or intravenous injection of biologically compatible solvents presaturated with polarized xenon. Additionally, the advantages and limitations of this method are described in light of a one-compartment xenon uptake/washout model.‖

BACKGROUND

To date, tissue delivery of polarized xenon has been performed using xenon respiration (9, 13, ¶). Respiration is ideally suited as a means of introducing polarized gases into the body for pulmonary studies, but it may be less efficient for certain studies involving remote organs, such as blood flow in the brain or muscular tissue. Recent simulations considering various physiological and experimental parameters have investigated the feasibility of using xenon respiration for such experiments by predicting the time-dependent concentration of polarized xenon in a chosen tissue (20, 21**).

One possible alternative to respiration delivery of polarized xenon is the localized injection of nontoxic solutions containing dissolved polarized xenon. Injection has been used as a means of delivering radioactive xenon isotopes (e.g., ^{133}Xe) to tissues for studies of muscular blood flow (22, 23). In circumstances where the invasiveness of injection is acceptable, polarized xenon injection would be advantageous when higher local concentrations of polarized xenon could be delivered to tissues relative to the concentration attainable by respiration. In the following, we adapt a simple, illustrative model to estimate the effective concentration of polarized xenon†† that could be delivered to tissues by direct injection.

Consider a one-compartment uptake/washout model using a bolus injection of an inert, freely diffusible tracer (polarized xenon) (see, for example, ref. 24). Such an injection could in principle be performed intravenously, intraarterially, or directly into the target organ. One can use the following relation

The publication costs of this article were defrayed in part by page charge payment. This article must therefore be hereby marked "*advertisement*" in accordance with 18 U.S.C. §1734 solely to indicate this fact.

Abbreviations: OP, optical pumping; MR, magnetic resonance.

‡Permanent address: School of Chemistry, Tel Aviv University, Tel Aviv 69978, Israel.

§To whom reprint requests should be addressed at: D-64 Hildebrand Hall, Department of Chemistry, University of California, Berkeley, CA 94720-1460. e-mail: pines@cchem.berkeley.edu.

¶Swanson, S. D., Rosen, M. S., Agranoff, B. W., Coulter, K. P., Welsh, R. C. & Chupp, T. E., 38th Experimental Nuclear Magnetic Resonance Conference, March 23–27, 1997, Orlando, FL.

‖This work was presented in part at the 38th Experimental Nuclear Magnetic Resonance Conference, March 23–27, 1997, Orlando, FL.

**An interactive web site containing a xenon respiration model can be found at http://ric.uthscsa.edu/staff/charlesmartinphd.html.

††The effective concentration of polarized xenon refers to the number of moles of 100% polarized, 100% isotopically labeled ^{129}Xe per unit volume, given an actual amount of xenon with known fractional polarization and isotopic labeling. For simplicity, we assume 100% isotopic labeling when using the model.

for the effective concentration C of polarized xenon in the targeted tissue following injection:‡‡

$$C(t) = \begin{cases} 0, & t \le T_d; \\ \dfrac{k_1 A}{k_2} \cdot e^{-T_d/T_{1s}^{Xe}} \cdot [1 - e^{-(t-T_d)k_2}], & T_d < t \le T_p; \\ C_{T_p} \cdot e^{-(t-T_p)k_2}, & T_p < t, \end{cases} \quad [1]$$

where k_1 is the specific volume flow in the tissue, k_2 is the effective washout rate defined by

$$k_2 = \left(\frac{k_1}{\lambda} + \frac{1}{T_1^{Xe}}\right); \quad [2]$$

(where λ is the tissue/blood partition coefficient), T_{1s}^{Xe} is the spin-lattice relaxation time of xenon in the solvent/blood environment, the peak time $T_p = T_d + T_i$, and C_{T_p} is the effective concentration of polarized xenon in the tissue at T_p. This model will be used to estimate expected NMR signal intensities after xenon injection.

MATERIALS AND METHODS

Detailed descriptions of both the polarized xenon injection technique (19) and the OP apparatus (25, 26) can be found elsewhere. Approximately 5×10^{-4} mol of isotopically enriched ^{129}Xe (80% ^{129}Xe; EG & G Mound, Miamisburg, OH) was placed in a glass cell with a small quantity of rubidium and was optically pumped with a 1.3-W Titan Ti:sapphire laser (continuous wave, 794.7 nm) for ≈30 min. The OP apparatus typically produces xenon samples with 5–10% nuclear polarization.

The remainder of the experimental procedure is shown schematically in Fig. 1. After OP, the xenon was frozen into the sidearm of the shaker in the presence of a magnetic field (50 mT) provided by a small permanent magnet. A delay of approximately 20 min between polarization and injection was necessary to transport the polarized xenon to the location of the imaging apparatus; however, the T_1 of solid xenon at the described magnetic field strength and temperature is on the order of hours (27). The xenon was sublimated and admitted to the degassed solvent [3 ml of 20% Intralipid emulsion (Pharmacia) or 3 ml of partially deuterated saline water, 0.9% by weight] under approximately 5 atm (1 atm = 101.3 kPa) of initial xenon pressure. In each experiment, 1 ml of the saturated xenon solution was withdrawn into a syringe through the rubber septum of the shaker prior to injection. NMR signal acquisition began at the start of the injection.

Male rats weighing 200–250 g were anesthetized intramuscularly with ketamine/xylazine/acepromazine (30/3/0.6 mg/kg), with supplemental doses administered as needed. For the spectroscopy experiment a venous catheter was placed into a tail vein, and the receiver/transmitter surface coil was placed over the heart and liver. For the imaging experiment a catheter was placed in the muscle of the rat's thigh and secured with tape, and the surface coil was placed over the injection site.

‡‡For simplicity, we treat the injection as a rectangular pulse transiting to the targeted region over a delivery time T_d with time extent T_i and constant concentration A, where $A = IV_i/PT_i$ (here I is the initial effective concentration of polarized xenon in the solvent, V_i is the total volume injected, and P is the flow rate between the site of injection and the target). This formulation assumes that $(V_i/T_i) < P$. If $(V_i/T_i) \ge P$, then $A = I$. If the polarized xenon solution is injected directly into the target tissue, then k_1 in Eq. **1** must be replaced by the injection rate divided by the tissue volume. This model assumes homogeneous and instantaneous equilibration of the xenon in the target tissue and that the effects of recirculation are rendered negligible by the short *in vivo* relaxation times and dilution of xenon throughout the body.

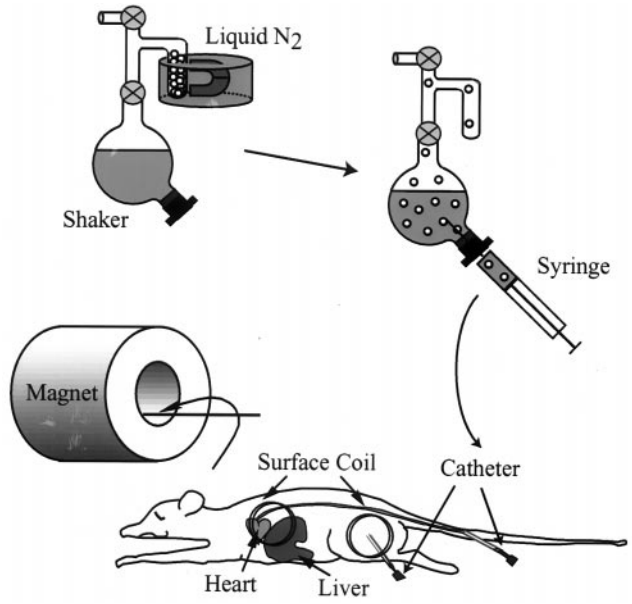

FIG. 1. Schematic of experimental procedure after OP. Before acquisition the sidearm of the shaker was removed from the liquid nitrogen and the polarized xenon was sublimated and admitted to the solution. After a brief period of vigorous shaking, the saturated xenon solution was withdrawn with a syringe and injected into a laboratory rat by means of a catheter.

Before each experiment the rat was placed in lateral recumbency into the magnet. Afterward the catheter was removed and the rat was returned to its cage to recover from anesthesia.

The ^{129}Xe magnetic resonance (MR) images and spectra were obtained on a home-built NMR spectrometer interfaced with a 2.35-T magnet (xenon frequency, 27.68 MHz; bore diameter, 25 cm). The receiver–transmitter surface coil had a diameter of 3.5 cm. For the spectroscopy experiment, spectra were obtained every second (pulse angle ≈ 20°). For the imaging experiment, axial images were acquired perpendicular to the coil by using the FLASH pulse sequence (28) shown in Fig. 2.

RESULTS AND DISCUSSION

Preliminary *in Vivo* Xenon Injection Experiments. In the spectroscopy experiment, a series of xenon NMR spectra were taken from the start of the intravenous injection of the xenon/Intralipid solution, with the detection coil placed over the heart/liver region. A sum of the spectra of the 7th through 12th scans is shown in Fig. 3; the time dependence of the individual spectra is shown in the *Inset*. The single resonance at about 190 ppm (downfield from a high-pressure xenon gas reference signal; see Fig. 3 legend) is consistent with xenon in the Intralipid (19). It was anticipated that the Intralipid would initially accumulate in the liver; it is likely that the initial rise in signal amplitude reflects this accumulation, while the subsequent decay is due to wash-out, relaxation, and magnetization loss from the application of the rf observation pulses.

In the imaging experiment, 10 two-dimensional ^{129}Xe MR images were taken at intervals of 6–7 s (with the exception of an 18-s delay between the fifth and sixth images) from the start of the injection of the xenon/saline solution. Six of these images are shown in Fig. 4, which depicts the signal intensity of the polarized xenon in the upper part of the rat's hind leg in near-axial cross section. The central region of lower xenon signal intensity (most visible in the second image) corresponds to the position of the rat's femur. From the six images, one may observe that the signal intensity first rises, reaching a maximum at the second image, and then decays. The initial rise in

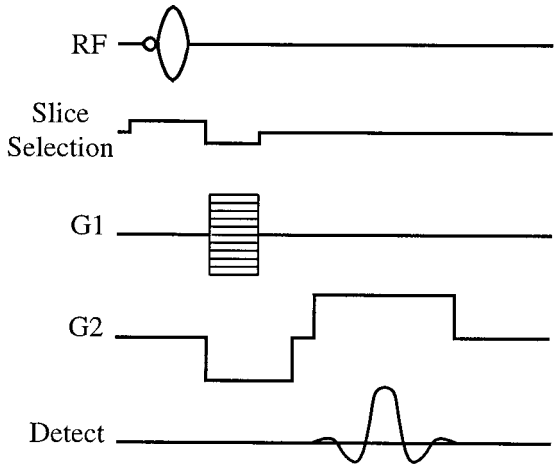

FIG. 2. The radiofrequency (RF) and gradient (G) pulse sequences for the FLASH (Fast Low-Angle SHot) imaging experiment. The following experimental parameters were used: tipping angle, ≈5°; pulse repetition time, 100 ms; slice thickness, 10 mm; field of view, 256 × 256 mm^2; acquisition matrix, 48 × 256.

intensity is due to the accumulation of the xenon/saline solution from the injection, while the subsequent decay is primarily due to the application of the rf pulses (48 pulses of approximately 5° tipping angle for each image), with relaxation and wash-out causing the secondary losses; the blood flow rate in muscle at rest is low, approximately equal to 2.12 ml/min per 100 g (29).

The major advantage of using saline water as the solvent is the long xenon T_1, which causes negligible loss of polarization over the injection time. However, the solubility of xenon in saline water is low, with an Ostwald coefficient of only 0.0926

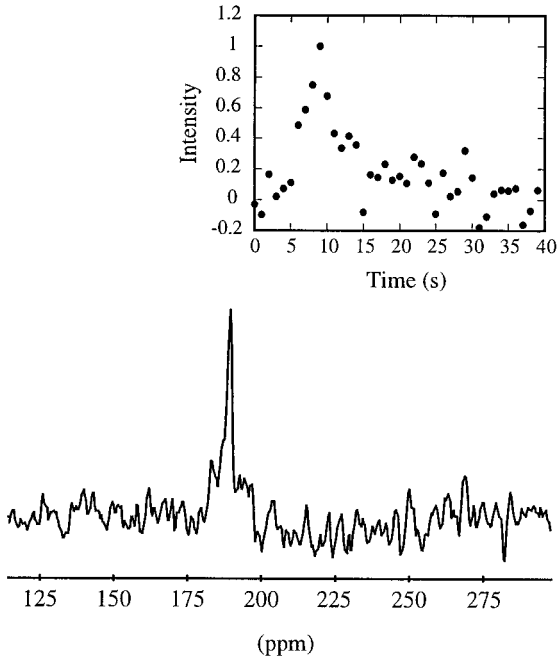

FIG. 3. ^{129}Xe spectrum obtained by summing the 7th through 12th scans of an injected xenon/Intralipid solution. The xenon/Intralipid solution was injected intravenously in the tail, and signal was acquired with a surface coil localized over the liver region. The chemical shift range is referenced to a polarized xenon gas sample (pressure ≈ 5 atm) scanned prior to experiment; the chemical shift is consistent with xenon residing in Intralipid once the reference pressure has been considered (19). (*Inset*) Time dependence of the integrated xenon signal in the liver region.

(the volume, at standard temperature and pressure, of xenon dissolved in 1 liter of liquid at 1 atm of gas pressure) (30). Higher xenon concentrations can be obtained with alternative xenon solvents [e.g., Intralipid and Fluosol (19, 31)], albeit at the expense of somewhat faster relaxation. For example, the T_1 of xenon in the Intralipid emulsion is about 40 s, whereas the T_1 of xenon in partially deuterated saline water is several hundred seconds (19). Furthermore, the xenon partitioning properties of such solvents in biological tissues may allow particular *in vivo* applications. Previous *in vitro* studies demonstrated that such solvents can bring about a 3-fold increase in the effective spin-lattice relaxation time of xenon in blood (19).

One clear disadvantage of using polarized xenon for tissue studies in general is the nonrenewable nature of the xenon polarization. Each acquisition destroys some of the polarization; the application of a pulse with tipping angle θ reduces the remaining longitudinal polarization by a factor of cos θ, and the spent polarization can be restored only by delivering fresh polarized xenon to the region being studied. This problem creates an additional difficulty for the imaging of polarized xenon, as the polarization loss incurred during the application of the rf pulses needed for multidimensional imaging can cause image blurring. It has been suggested that this problem can be avoided by using pulse sequences that use variable tip-angle pulses to maintain signal amplitude during image acquisition (32, 33).

The loss of polarization after each acquisition during blood-flow studies may also make accurate measurement of perfusion rates difficult, a problem that can be appreciated by examining the signal decay in Fig. 4. If the signal loss from image to image due to rf pulse application is significant with respect to that due to wash-out, highly accurate pulse calibration would be critical to extracting the intrinsic wash-out rate from the observed rate of signal loss. Two possible methods that may be applicable in such circumstances for calibrating the tipping angle of an arbitrary pulse are discussed in ref. 33. However, signal loss due to pulsing would not likely affect chemical-shift studies.

Predictions of the Model. Previous models of polarized xenon respiration were designed for brain studies, motivated by a variety of possible biomedical applications [e.g., brain blood flow and demyelination studies (20, 21)]. To compare the injection method with xenon respiration, one can use the model described by Eq. **1** to estimate the peak effective polarized xenon concentration in the brain after an intracarotid injection of a polarized xenon/Intralipid solution. Using Eq. **1** and the parameter values summarized in Table 1, one can estimate a peak polarized xenon concentration of about 7×10^{-2} mM at $T_p = 5$ s. This concentration could be increased with better initial xenon polarization, the injection of more solution, greater xenon overpressure in the shaker, or by using a biologically compatible solvent with a greater xenon solubility. However, this calculation does not consider certain complicating physiological issues, such as the differing perfusion rates, xenon solubilities, and xenon relaxation times of different brain tissues. As k_2 is approximately 0.043 s^{-1}, the xenon concentration will decay with a time constant of about 23 s after T_p. Thus, even when the targeted organ has a relatively high rate of blood flow, the contribution from rf-induced polarization loss to the observed signal decay rate would likely be significant in a perfusion imaging experiment.

In comparison to the estimated peak polarized xenon concentration of 7×10^{-2} mM for an intracarotid injection, models of respiration tissue delivery of polarized xenon predict peak concentrations that are severalfold less. For example, using the interactive model of Martin (21), one can obtain a peak polarized xenon concentration in the brain of 8.2×10^{-3} mM after a single held breath composed of 80% xenon with the same polarization. (This value was calculated using the same

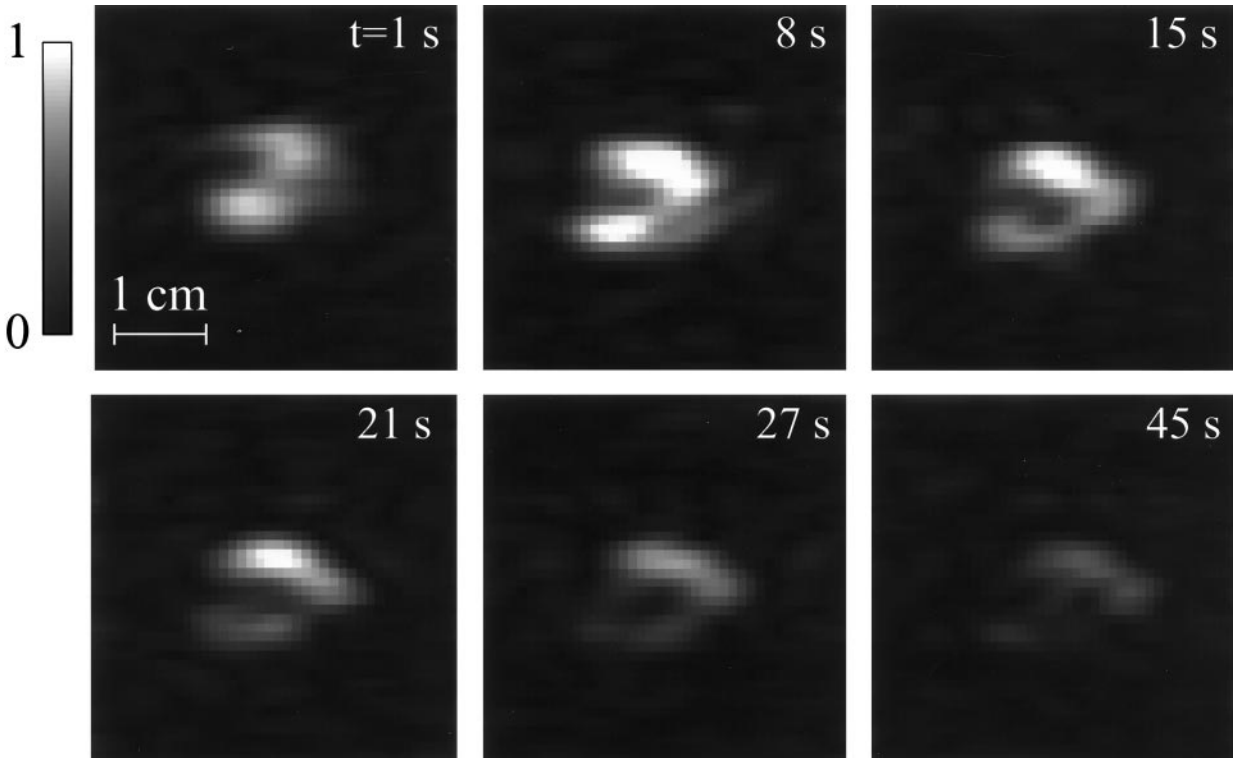

FIG. 4. ^{129}Xe MR images of an optically pumped xenon/saline solution injected into the upper hind leg of a living rat. Acquisitions began immediately after the beginning of an injection period of a few seconds, and they were taken at 1, 8, 14, 21, 27, and 45 s. Displayed image intensities were normalized to the second image. The sixth image was the first of the second series of acquisitions; the signal remained strong enough to be seen through the final acquisition, 70 s into the experiment. The peak signal-to-noise ratio, achieved in the second image, is about 16:1, and the ratio drops to about 8:1 in the sixth image. Images were acquired by using the FLASH sequence as shown in Fig. 2. Images as shown were prepared by zero-filling to give a 256 × 256 matrix and by applying a 50-Hz Gaussian apodization along the frequency-encoding dimension.

experimental and physiological parameter values as those used in our estimate, excepting those related exclusively to respiration, for which the model's default values were used.) Continuous breathing of a 35% xenon mixture [whose xenon concentration would be low enough to prevent anesthetic effects (36)] would yield a peak polarized xenon concentration of 3.3×10^{-3} mM. The increase in peak polarized xenon concentration estimated for injection delivery from that predicted for respiration is primarily due to rapid and localized delivery, high initial concentration (i.e., xenon solubility in Intralipid), and extended *in vivo* xenon relaxation time. However, it must be mentioned that the polarized xenon concentrations predicted by both our simple estimate and the respiration models depend greatly upon the values of experimental and physiological parameters, some of which are not known with a high degree of accuracy for all physiological conditions.

Table 1. Parameter values used for xenon injection model

Parameter	Value
V_i	5 ml
T_i	3 s
I	8.7 mM*
k_1	[0.00917 s^{-1}]†
P	4.9 ml/s‡
λ	1§
T_{1s}^{Xe}	16 s¶
T_1^{Xe}	30 s‖
T_d	2 s

*Estimated from the relative solubility of xenon in the Intralipid emulsion (19), and assuming a 5-atm equilibrium xenon overpressure, an initial xenon polarization of 0.1, and 100% isotopic labeling.
†From a brain blood flow rate of 52.9 ml/min per 100 g (ref. 29), a brain mass of 1,400 g, and a specific gravity of 1.04 (ref. 34).
‡Estimated as the total volume of blood per second supplied by one carotid artery, given the value for k_1.
§Effective value estimated from those of white and gray matter given in ref. 35 (*in vitro* data from dogs).
¶From ref. 19.
‖From ¶ footnotes in text, in rat brain.

The respiration techniques are well suited for cardiopulmonary applications, and they have the advantage of being noninvasive. However, they require preparation of large amounts of polarized xenon gas. On the other hand, the injection technique is by its nature invasive, but it requires a far smaller amount of polarized xenon, which may be an important consideration in light of the cost and local availability of laser-polarized isotopically enriched ^{129}Xe. Furthermore, in some circumstances it may be required to reduce the amount of xenon in the breathing mixture used in the respiration method to avoid unwanted anesthetic effects, as the concentration of relaxed xenon in the brain during such experiments would be significantly higher than the effective polarized xenon concentration (21). However, because of the invasive nature of intraarterial injection, the arterial route is not appropriate for routine clinical applications.

Even when circumstances present an advantage of using xenon injection over respiration (i.e., when the local perfusion rate is low, the transit time of blood from the lungs to the target region is long, and the danger from invasive injections is relatively low, such as for studies involving muscular tissue) the observable signal intensity from the polarized xenon will still be generally inferior to that of tissue protons. Consider a best-case scenario in which the xenon has been polarized to 50%. When the previous example of injection delivery of xenon to the brain is used, a peak polarized xenon concentration of about 0.3 mM would be obtained, yielding ≈30% of the NMR signal-to-noise from protons in a 1-T magnet (recall that the concentration of protons in the body is ≈80 M, their

polarization in a 1-T field is $\approx 3.2 \times 10^{-6}$, and the relationship between the proton and ^{129}Xe magnetogyric ratios is $\gamma_H \approx 3.61\gamma_{Xe}$).

The promise of polarized xenon lies primarily in its large chemical-shift range [≈200 ppm when dissolved in various solutions (37)], derived from xenon's high polarizability. It is hoped that xenon's sensitivity to its local magnetic environment will enable novel *in vivo* localized NMR spectroscopy and chemical-shift imaging experiments. Additionally, high local concentrations of polarized xenon may permit the differential measurement of polarization transfer to other nuclear spins (38) in the body, providing a novel means of contrast on both the macroscopic and molecular level. These effects have been shown to be larger and site-selective in molecules that hydrophobically interact with xenon (39).

CONCLUSION

This report contains MR images and spectra taken of polarized xenon injected directly into the tissues of living organisms. While it is believed that in general polarized xenon may be useful for a number of biomedical applications such as MRI angiography and perfusion imaging, the injection of polarized xenon solutions is particularly promising for *in vivo* localized NMR spectroscopy and chemical-shift imaging. By using injection, one can administer polarized xenon rapidly, locally, and efficiently, especially if the experimental situation has an indication for intraarterial or intramuscular injections. Specifically, under conditions where unique information regarding disease mechanisms can be revealed by NMR spectroscopy, injections of polarized xenon may have substantial medical science benefits in human studies regarding the nature of healthy and pathological tissues.

We thank Tom Lawhead for his expert glassblowing and advice. We also thank Dr. Scott Swanson for helpful discussions regarding polarized xenon in the brain and Dr. Charles Martin for helpful discussions regarding his xenon respiration model. We also thank Dr. Michael Weiner for helpful comments regarding the manuscript. Y.-Q.S. acknowledges a research fellowship from the Miller Institute for Basic Research in Science. This work was supported by the Director, Office of Basic Sciences, Materials Sciences Division of the U.S. Department of Energy under Contract DE AC03–76SF00098.

1. Kastler, A. (1950) *J. Phys. Radium* **11,** 255–265.
2. Bouchiat, M. R., Carver, T. R. & Varnum, C. M. (1960) *Phys. Rev. Lett.* **5,** 373–375.
3. Happer, W., Miron, E., Schaefer, S., Schreiber, D., von Wijngaarden, W. A. & Zeng, X. (1984) *Phys. Rev. A* **29,** 3092–3110.
4. Albert, M. S., Cates, G. D, Driehuys, B., Happer, W., Saam, B., Springer, C. S., Jr., & Wishnia, A. (1994) *Nature (London)* **370,** 199–201.
5. Middleton, H., Black, R. D., Saam, B., Cates, G. D., Cofer, G. P., Guenther, R., Happer, W., Hedlund, L. W., Johnson, G. A., Juvan, K. & Swartz, J. (1995) *Magn. Reson. Med.* **33,** 271–275.
6. Black, R. D., Middleton, H. L., Cates, G. D., Cofer, G. P., Driehuys, B., Happer, W., Hedlund, L. W., Johnson, G. A., Shattuck, M. D. & Swartz, J. C. (1996) *Radiology* **199,** 867–870.
7. Macfall, J. R., Charles, H. C., Black, R. D., Middleton, H., Swartz, J. C., Saam, B., Driehuys, B., Erickson, C., Happer, W., Cates, G. D., Johnson, G. A. & Ravin, C. E. (1996) *Radiology* **200,** 553–558.
8. Leduc, M. & Otten, E. (1996) *La Recherche* **287,** 41–43.
9. Sakai, K., Bilek, A. M., Oteiza, E., Walsworth, R. L., Balamore, D., Jolesz, F. & Albert, M. S., (1996) *J. Magn. Reson. B* **111,** 300–304.
10. Wagshul, M. E., Button, T. M., Li, H. F., Liang, Z., Springer, C. S., Jr., Zhong, K. & Wishnia, A. (1996) *Magn. Reson. Med.* **36,** 183–191.
11. Bachert, P., Schad, L. R., Bock, M., Knopp, M. V., Ebert, M., Grossman, T., Heil, W., Hofmann, D., Surkau, R. & Otten, E. W. (1996) *Magn. Reson. Med.* **36,** 192–196.
12. Kauczor, H. U., Hofmann, D., Kreitner, K. F., Nilgens, H., Surkau, R., Heil, W. Potthast, A., Knopp, M. V., Otten, E. W. & Thelen, M. (1996) *Radiology* **201,** 564–568.
13. Mugler, J. P. III, Driehuys, B., Brookeman, J. R., Cates, G. D., Berr, S. S., Bryant, R. G., Daniel, T. M., del Lange, E. E., Downs, J. H. III, Erickson, C. J., Happer, W., Hinton, D. P., Kassel, N. F., Maier, T., Phillips, C. D., Saam, B. T., Sauer, K. L. & Wagshul, M. E. (1997) *Magn. Reson. Med.* **37,** 809–815.
14. Albert, M. S., Tseng, C. H., Williamson, D., Oteiza, E. R., Walsworth, R. L., Kraft, B., Kacher, D., Holman, B. L. & Jolesz, F. A. (1996) *J. Magn. Reson. B* **111,** 204–207.
15. Song, Y.-Q., Gaede, H. C., Pietrass, T., Barrall, G. A., Chingas, G. C., Ayers, M. R. & Pines, A. (1995) *J. Magn. Reson. A* **115,** 127–130.
16. Raftery, D. & Chmelka, B. (1994) in *NMR Basic Principles and Progress*, eds. Diehl, P., Fluck, E., Günther, H., Kosfeld, R. & Seelig, J. (Springer, Berlin), Vol. 30, pp. 111–158.
17. Kennedy, R. R., Stokes, J. W. & Downing, P. (1992) *Anaesth. Intens. Care* **20,** 66–70.
18. Albert, M. S., Schepkin, V. D. & Budinger, T. F. (1995) *J. Comput. Assist. Tomogr.* **19,** 975–978.
19. Bifone, A., Song, Y.-Q., Seydoux, R., Taylor, R. E., Goodson, B. M., Pietrass, T., Budinger, T. F., Navon, G. & Pines, A. (1996) *Proc. Natl. Acad. Sci. USA* **93,** 12932–12936.
20. Peled, S., Jolesz, F. A., Tseng, C. H., Nascimben, L., Albert, M. S. & Walsworth, R. L. (1996) *Magn. Reson. Med.* **36,** 340–344.
21. Martin, C. C., Williams, R. F., Gao, J. H., Nickerson, L. D. H., Xiong, J. & Fox, P. T. (1997) *J. Magn. Reson. Imaging* **7**, 848–854.
22. Lassen, N. A., Lindbjerg, J. & Munck, O. (1964) *Lancet* **i,** 686–689.
23. Pozderac, R. V., Miller, T. A. & Lindenauer, S. M. (1975) *Radiology* **117,** 633–635.
24. Budinger, T. F. & Huesman, R. H. (1985) *Circulation* **72,** 53–62.
25. Raftery, D., Long, H., Meersmann, T., Grandinetti, P. J., Reven, L. & Pines, A. (1991) *Phys. Rev. Lett.* **66,** 584–587.
26. Pietrass, T. & Gaede, H. C. (1995) *Adv. Mat.* **7,** 826–838.
27. Gatzke, M., Cates, G. D., Driehuys, B., Fox, D., Happer, W. & Saam, B. (1993) *Phys. Rev. Lett.* **70**, 690–693.
28. Haase, A., Frahm, J., Matthaei, D., Hanicke, W. & Merboldt, K. D. (1986) *J. Magn. Reson.* **67,** 258–266.
29. Cowles, A. L., Borgstedt, H. H. & Gillies, A. J. (1971) *Anesthesiology* **35,** 523–526.
30. Isbister, W. H., Schofield, P. F. & Torrance, H. B. (1965) *Phys. Med. Biol.* **10,** 243–250.
31. Beauregard, D. (1995) *Chem. Ind. (London)* **12,** 459–460.
32. Zhao, L., Mulkern, R., Tseng, C.-H., Williamson, D., Patz, S., Kraft, R., Walsworth, R. H., Jolesz, F. A. & Albert, M. S. (1996) *J. Magn. Reson. B* **113,** 179–183.
33. Patyal, B. R., Gao, J.-H., Williams, R. F., Roby, J., Saam, B., Rockwell, B. A. Thomas, R. J., Stolarski, D. J. & Fox, P. T. (1997) *J. Magn. Reson.* **126,** 58–65.
34. Snyder, W. S., chair of Task Group Reference Man (1975) *Ann. ICRP* **23,** 121.
35. Chen, R. Y. Z., Fan, F.-C., Kim, S., Jan, K.-M., Usami, S. & Chien, S. (1980) *J. Appl. Physiol.* **49,** 178–183.
36. Bidabé, A. M., de Beaufort, D. G., Gin, A. M. & Caillé, J. M. (1990) *J. Neuroradiol.* **17,** 103–124.
37. Miller, K. W., Reo, N. V., Uiterkamp, A. J. M. S., Stengle, D. P., Stengle, T. R. & Williamson, K. L. (1981) *Proc. Natl. Acad. Sci. USA* **78,** 4946–4949.
38. Navon, G., Song, Y.-Q., Rõõm, T., Appelt, S., Taylor, R. E. & Pines, A. (1996) *Science* **271,** 1848–1851.
39. Song, Y.-Q., Goodson, B. M., Taylor, R. E., Laws, D. D., Navon, G. & Pines, A. (1997) *Angew. Chem.* **109**, 2464–2466.